ChemComm

Accepted Manuscript

This article can be cited before page numbers have been issued, to do this please use: D. Wang, B. Ma, B. Wang, C. Zhao and P. WU, *Chem. Commun.*, 2015, DOI: 10.1039/C5CC06212H.

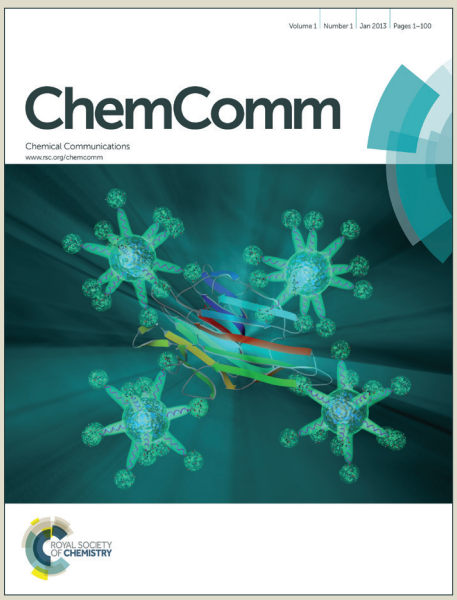

ROYAL SOCIETY OF CHEMISTRY

www.rsc.org/chemcomm

View Article Online
DOI: 10.1039/C5CC06212H

Graphic Abstract

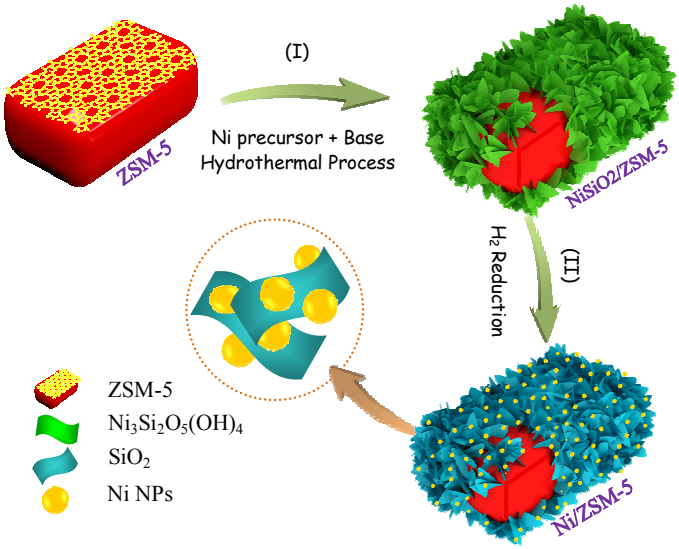

One-pot synthesis of hierarchical zeolite supported metal nanoparticle catalysts are realized through a base-assisted chemoselective interaction.

View Article Online
DOI: 10.1039/C5CC06212H

Journal Name

COMMUNICATION

One-Pot Synthesized Hierarchical Zeolites Supported Metal Nanoparticles for Highly Efficient Biomass Conversion†

Received 00th January 20xx,
Accepted 00th January 20xx

DOI: 10.1039/x0xx00000x

www.rsc.org/

Darui Wang, Bing Ma, Bo Wang, Chen Zhao* and Peng Wu*

Hierarchically porous zeolites supported metal nanoparticles are successfully prepared through a base-assisted chemoselective interaction between the silicon species on zeolite crystal surface and metal salts, in which in-situ construction of mesopores and high dispersion of metal species are realized simultaneously.

Synthetic zeolites with well-defined crystalline structures, unique microporosity and high surface areas have attracted technological and scientific research attentions in the adsorption, separation and catalysis fields.[1] Supporting metal nanoparticles (NPs) on zeolites, preferably with stable characters and uniform nanosize, leads to useful catalysts for F-T synthesis,[2] CO oxidation,[3] hydroisomerization[4] and hydrodeoxygenation etc.[5-7] It is well acceptable that the physiochemical properties and catalytic activity of NPs are superior to those of bulk metals. However, smaller NPs tend to aggregate because of a large surface area-to-volume ratio, which greatly limits their actual applications.[8-10] The preparation method is thus an important factor dominating the catalytic properties and performances of metal NPs catalysts.

Wetness impregnation (IM) is a simple preparation technique widely used in the industrial process. However, metal-based catalysts prepared by conventional IM procedure encounters the drawbacks of large and non-uniform metal particles as the metal-support interaction is relatively weak for silica-based zeolite supports,[11] leading to low metal dispersion and unsatisfied catalytic activity.[6,12] On the other hand, the ion-exchange process can obtain small metal particles with a higher dispersion, but the metal loading amount is limited by the exchange capacity of zeolites.[13] Metal-based catalyst has also been prepared by sol-gel method. For example, Ueno and co-workers prepared Ni/SiO_2 from tetraethoxysilane (TEOS) and nickel nitrate by using ethylene glycol as either a solvent or a ligand for nickel.[14] Unfortunately, the nickel particle size becomes larger than 10 nm when its loading is over 10 wt%.[15] The deposition-precipitation (DP) method developed by Geus et al.[16] is promising to achieve a high metal dispersion at relatively high loadings. In order to improve the catalytic properties and to shorten the preparation time, the amount of metal compound added in initial solution often greatly exceeds that of actually loaded on supports.[6,17-19] Therefore, it is highly expected to develop eco-efficient approaches for achieving highly dispersed and stable metal NPs at high loadings.

Hierarchical materials are known to serve as good supports for dispersing and stabilizing metal NPs or other coordinate compounds. Recently, great efforts have been devoted to the design and controlled fabrication of hierarchical materials with novel structures.[20-25] For instance, Jin *et al*. once prepared copper-silicate hollow fibers with a ultra small nanotube-assembled and double-walled structure.[26] The as-prepared hollow fibers possess mesopores centered at 3.4 nm and high surface area, and they exhibit an excellent performance as an ideal support for noble metal catalysts. Recently, we have prepared core-shell structured ZSM-5@mesosilica and further incorporated Pt NPs into the mesosilica shell, resulting in an effective catalyst towards n-hexadecane hydrocracking. Generally, the preparing procedures for hierarchical materials are inevitably complicated, and additional steps are required to confine the metal NPs in mesopores.

Herein, we communicate a facile route for synthesizing hierarchical ZSM-5 supported Ni NPs starting from conventional crystals. The construction of flower-like hierarchical ZSM-5 structure and incorporation of highly dispersed and stable Ni active sites are accomplished in one pot. The obtained Ni/ZSM-5 catalysts are highly efficient to the hydrodeoxygenation of bioacids to liquid fules.

As illustrated in Scheme 1, in the first step, the flower-like nickel silicate precursors were chemically formed and coated on the polycrystalline particles of zeolite via base-assisted chemoselective interaction with corresponding metal source.

Shanghai Key Laboratory of Green Chemistry and Chemical Process, School of Chemistry and Molecular Engineering, East China Normal University , North Zhongshan Rd. 3663, Shanghai 200062, China
E-mail: pwu@chem.ecnu.edu.cn, czhao@chem.ecnu.edu.cn;
Fax: (+)86-21-62232292
†Electronic Supplementary Information (ESI) available: Details of experimental procedures and material characterization. See DOI: 10.1039/x0xx00000x

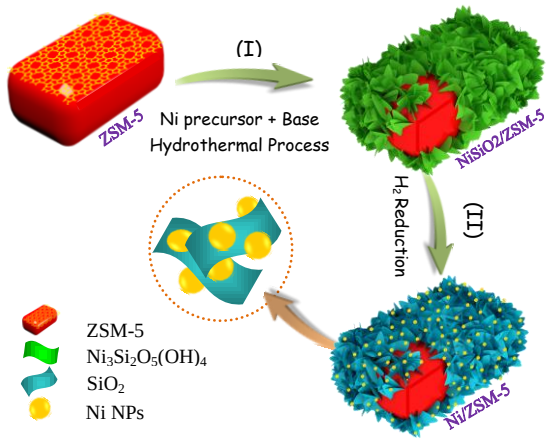

Scheme 1 Schematic illustration of the preparation procedures for Ni nanoparticles supported on hierarchical ZSM-5 zeolite crystals.

This process involved the selective and partial dissolving of silica species off the ZSM-5 crystals to form silicate anions and then in situ interaction with the nickel cations in solution to form the layered nickel silicate, giving rise to a composite material $NiSiO_2$/ZSM-5. The hydrothermal reaction between SiO_2 and Ni^{2+} took place as follows: $2SiO_2 + 3Ni^{2+} + 5H_2O = Ni_3Si_2O_5(OH)_4 + 6H^+$.[28] Secondly, the nickel silicate precursors underwent decomposition and reduction in a hydrogen atmosphere. The remaining SiO_2 matrixes still maintaining flower-like structure, whereas highly dispersed Ni NPs were immobilized therein, obtaining Ni/ZSM-5 catalyst. This novel host-guest method is featured by the simultaneous construction of hierarchical zeolite structure and confined metal NPs.

Well-structured $NiSiO_2$/ZSM-5 materials were prepared readily by hydrothermal reaction under optimal temperature and time of 120 °C and 3 h (Fig. S1 and S2, ESI†). The supporting of highly dispersed Ni NPs on hierarchical ZSM-5 by this novel method has been traced with the XRD patterns and FT-IR spectra. The XRD pattern of the pristine ZSM-5 was characteristic of a typical MFI structure (Fig. 1a). After the hydrothermal treatment in nickel acetate-containing solution, the resultant $NiSiO_2$/ZSM-5 showed additional XRD diffractions around 34.1°, 36.7° and 60.5° in high angle region (Fig. 1b), which are indexed as the [200], [202] and [060] planes of nickel silicate ($Ni_3Si_2O_5(OH)_4$, JCPDS No. 49-1859).[29] Fig. displays the XRD pattern of Ni/ZSM-5 after reduction. The weak peaks centered at 44.5° and 51.8°, corresponding to the [111] and [200] planes of cubic Ni (JCPDS No. 04-0850),[30] were observed with the disappearance of nickel silicate phase. The results indicated that the Ni species in layered nickel silicate were converted into metal Ni particles by H_2 reduction at high temperature. FT-IR spectroscopy was utilized to detect the formed functional groups. A new band emerged for $NiSiO_2$/ZSM-5 at around 670 cm^{-1} (Fig. S3, ESI†), which is ascribed to the Si-O-Ni stretching vibrations.[31] This further verified the formation of nickel silicate precursors after hydrothermal reaction. This band disappeared for Ni/ZSM-5 after H_2 reduction, reasonably because that the Si-O-Ni linkages were broken instead of forming Ni NPs.

The morphology, structure, and composition of the samples obtained at different stages were investigated by various characterization techniques. The SEM image shows that the pristine ZSM-5 was of the polycrystalline particles with relatively smooth surface and a regular size of 1 - 2 µm (Fig. 2a). After hydrothermal treatment with Ni source, the as-fabricated $NiSiO_2$/ZSM-5 precursors retained almost the original crystal shape and size (Fig. 2b). Careful observation by

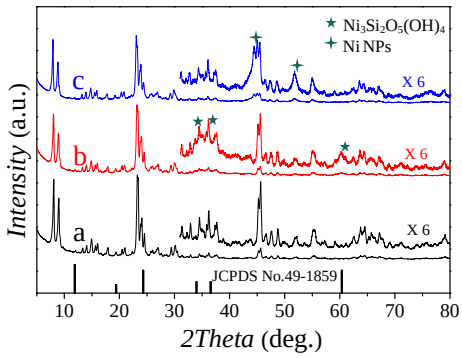

Fig. 1 XRD patterns of the pristine ZSM-5 (a), $NiSiO_2$/SM-5 (b), Ni/ZSM-5 (c) and nickel silicate.

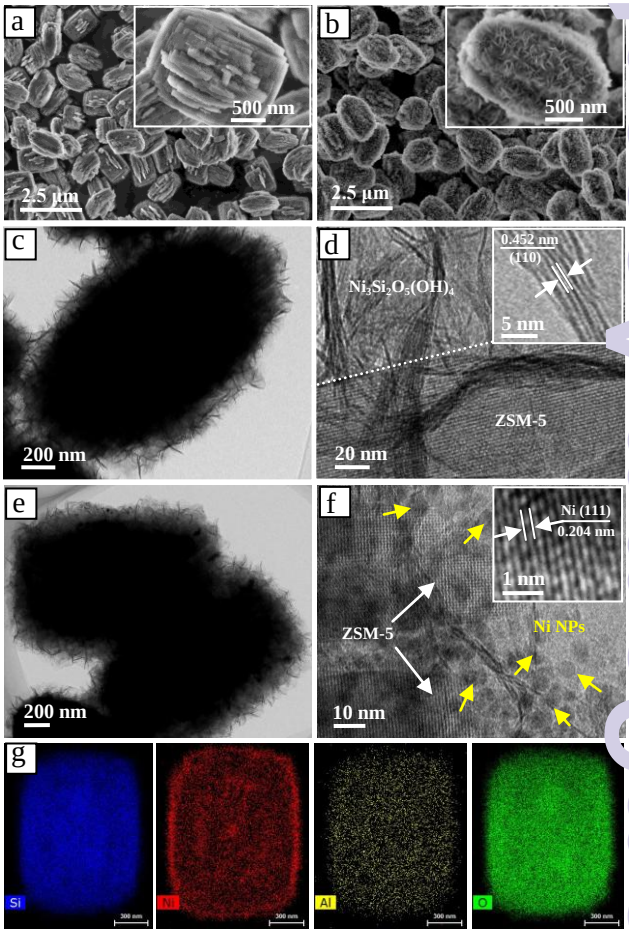

Fig. 2 SEM images of pristine ZSM-5 (a) and $NiSiO_2$/ZSM-5 (b); TEM images of $NiSiO_2$/ZSM-5 (c, d) and Ni/ZSM-5 (e, f); and elemental mapping of $NiSiO_2$/ZSM-5 (g).

the high-magnification SEM image indicated that the surface of these precursors was no longer smooth but composed of numerous nanosheets (Fig. 2b, inset). The TEM image (Fig. 2c) clearly displays that the precursors possessed a typical core/shell like structure, with flexible nanosheets uniformly coating on the ZSM-5 crystals. A representative high-resolution TEM image indentified clearly that the composite materials contained the flower-like nanosheets and the crystalline ZSM-5 crystal, confirming the presence of a core/shell structure (Fig. 2d). The inset in Fig. 2d and Fig. S4 (ESI†) show the enlarged image of nanosheets, indicating they possessed a layered structure. The distance of the adjacent lattice fringes was determined to be about 0.452 nm and 0.153 nm, corresponding well to the d_{110} and d_{060} spacing of $Ni_3Si_2O_5(OH)_4$ (JCPDS No. 49-1859), respectively. Elemental mapping by energy-dispersive X-ray spectroscopy (EDX) verified that the elements Si, Al, O, Ni were homogeneously distributed throughout the whole single particle (Fig. 2g). This implies that a high dispersion of Ni NPs would be achieved after thermal reduction. In addition, a similar hydrothermal treatment without using Ni source was also done, Fig. S5 (ESI†) shows that the treated ZSM-5 have the same morphological features and textural properties as the pristine ZSM-5, which means the microporous characteristics of the core.

The TEM images (Fig. 2e) and SEM images (Fig. S6, ESI†) indicated that the reduced samples of Ni/ZSM-5 also showed a good core/shell structure, as the remaining silica parts still existed as shell matrixes after decomposition of nickel silicate precursors. The spherical Ni NPs were dispersed uniformly on the SiO_2 matrixes, just like "diamond on the beach" (Fig. S7, ESI†). In the HRTEM image (Fig. 2f), the spherical Ni NPs of about 5 nm can be easily observed. The distance of the adjacent lattice fringes in NPs was determined to be about 0.204 nm, corresponding well to the d_{111} spacing of cubic Ni (JCPDS No. 04-0850).[32]

To demonstrate the synthetic controllability, the products were synthesized with different nickel contents, corresponding to theoretical loading amounts of 7.5, 10.0, 20.0 and 30.0 wt%. ICP analyses indicated the Ni contents actually loaded on zeolite were 7.6, 10.3, 20.4 and 30.6 wt%, respectively. Thus, this method gave a utilization efficiency of nickel source close to 100 % and easily controlled the Ni loading amounts in a relatively wide range.

Fig. S8 (ESI†) shows the SEM images of $NiSiO_2$/ZSM-5 with different nickel contents. At lower Ni loadings of 7.6 wt% and 10.3 wt%, although small amounts of flower-like nanosheets were assembled on the ZSM-5 crystals, the rough surfaces were already observed clearly. Certainly, larger amount nanosheets were formed when the nickel contents reached 20.4 wt% and 30.6 wt%. Fig. S9 (ESI†) gives the corresponding SEM images of Ni/ZSM-5. The amounts of remaining SiO_2 matrixes increased with an increasing nickel content, as more nickel silicate precursors were decomposed and reduced. The HRTEM images verified that ultrafine Ni NPs were well dispersed among the SiO_2 matrixes independent of high nickel loadings (Fig. S10, ESI†). The particle size was still centered at about 6.0 nm even at a high loading of 30.6 wt% (Fig. S10d, inset, ESI†). This synthetic method has an obvious advantage that the monodispersed Ni NPs do not clump together at ultra high loadings.

The N_2 adsorption/desorption isotherms and pore size distribution are shown in Fig. S11 (ESI†). After introducing Ni NPs, Ni/ZSM-5 showed the isotherms combining type I and type IV characters, indicating the presence of both micropores and mesopores. The pore size distribution showed that Ni/ZSM-5 possessed the mesopores with 5 - 30 nm diameter. The mesopores are mainly ascribed to the disordered assembly of the flexible SiO_2 matrixes. The mesopore surface areas increased from 25 $m^2\ g^{-1}$ to 126 $m^2\ g^{-1}$ and mesopore volumes increased from 0.08 $cm^3\ g^{-1}$ to 0.29 $cm^3\ g^{-1}$ when 30.6 wt% Ni was incorporated into ZSM-5 (Table S1, ESI†). These novel materials, with confined space and enhanced mass transfer rate, would have potential applications as bifunctional catalysts.

The acidity of pristine ZSM-5 and Ni/ZSM-5 was investigated by pyridine-IR (Fig. S12, ESI†). Compared with ZSM-5, Ni/ZSM-5 possessed slightly lower concentration of Brønsted acid sites and higher concentration of Lewis acid sites. Those ionic Ni species, partially unreduced as evidenced by H_2-TPR investigation (Fig. S13, ESI†), are speculated to be the potential Lewis acid sites.[33] The state of Al was also investigated by ^{27}Al MAS NMR (Fig. S14, ESI†), the microenvironment of Al became more asymmetric in coordination states after incorporating nickel content.

The Ni/ZSM-5 catalyst was evaluated in the conversion of biomass to fuel using hydrodeoxygenation of stearic acid with H_2 at 260 °C and 4 MPa. Fig. 3a presents the conversion of the stearic acid over Ni/ZSM-5 with different Ni loadings. The conversion of stearic acid increased from 39.2% to 86.1% at 60 min, as the Ni loading was increased from 7.6 wt% to 30.6 wt%. Accordingly, the reaction rate increased from 34 to 44, 69 and 76 mmol $g^{-1}\ h^{-1}$ (Table S3, ESI†). A kinetic curve revealed that the reaction took place proportionally to the time, giving *n*-C18 alkanes as major products (Fig. S15, ESI†).

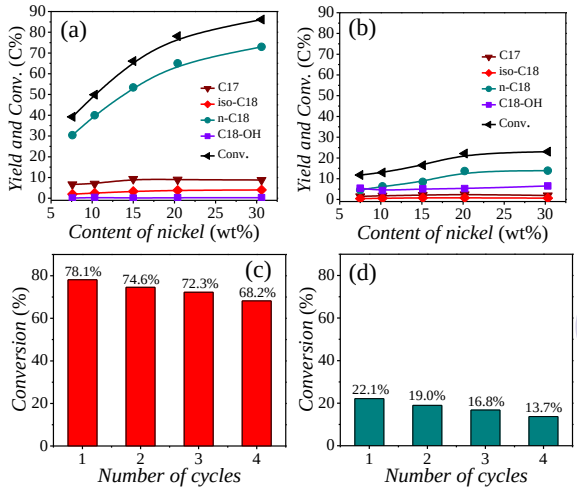

Fig. 3 Yield and conversion for stearic acid hydrodeoxygenation over Ni/ZSM-5 (a) and IM-Ni/ZSM-5 (b) with different Ni contents; stability tests for the Ni/ZSM-5 (c) and IM-Ni/ZSM-5 (d) catalysts, Ni contents are about 20.4 wt% and 20.2 wt%, respectively. Reaction conditions: 5.0 g stearic acid, 0.2 g catalyst, 80 mL dodecane, 260 °C, 4 MPa H_2, 60 min, stirring at 600 rpm.

IM-Ni/ZSM-5 with different Ni contents was synthesized by wetness impregnation for comparison. It is obvious that the catalytic activity of IM-Ni/ZSM-5 was much lower than that of Ni/ZSM-5 when compared at the same Ni loadings (Fig. 3b). The textural properties and the size of Ni NPs were considered to contribute the high catalytic activity. Compared with Ni/ZSM-5, IM-Ni/ZSM-5 showed no increase in mesopore surface area or mesopore volume (Fig. S16 and Table S2, ESI†) and possessed larger Ni NPs with an average diameter of 30 nm (Fig. S17, ESI†). The CO chemisorption measurement evidenced that Ni/ZSM-5 contained more highly dispersed Ni NPs than IM-Ni/ZSM-5 (Table S3, ESI†).

In a following step, the stabilities of Ni/ZSM-5 and IM-Ni/ZSM-5 were checked by recycling the catalyst. No notable changes in activity were observed over four cycles for Ni/ZSM-5 (Fig. 3c), the stearic acid conversion dropped slightly from 78.1% to 68.2%. However, IM-Ni/ZSM-5 lost about 40% of its initial activity after four reaction runs (Fig. 3d). The activity loss was presumed mainly due to the aggregation of Ni NPs during the successive reaction. For the reused Ni/ZSM-5 catalyst, the morphology maintained well, and the average diameters of Ni particles were still much smaller than that of the reused IM-Ni/ZSM-5 (Fig. S18, ESI†). To undertake a deeper investigation into this issue, the stability was further checked by treating the catalysts at 800 ^{o}C for 24 h in a flow of H_2. Ni/ZSM-5 demonstrated a much higher stability against sintering with slight increase of Ni particles size (Fig. S19a, ESI†).

Importantly, the synthetic strategy described above is quite general. We have successfully prepared other bifunctional catalysts by simply varying types of zeolites or metal salts in the hydrothermal reaction, such as Ni/MOR, Ni/Beta, Ni/HY, Ni/MCM-22, Cu/ZSM-5 and Co/ZSM-5 (Fig. S20-22, ESI†).

In summary, we have developed a facile route for preparing well-dispersed metal NPs supported on hierarchical zeolites, in which mesopores and metal active sites can be incorporated in one pot. The as prepared Ni/ZSM-5 catalysts exhibit excellent catalytic activity and stability in the hydrodeoxygenation of bioacid. The mesoporous SiO_2 matrixes effectively prevent the Ni NPs from sintering. In particular, the synthetic strategy provides an useful idea for controllable supporting of other metal NPs on different zeolites, and gives rise to promising bifunctional catalysts for industrial processes, such as F-T synthesis, hydrocracking, hydroisomerization and hydrodeoxygenation etc.

The authors gratefully acknowledge the financial supports from NSFC of China (21533002 and 21373089), Ministry of Science and Technology (2012BAE05B02), Programs Foundation of Ministry of Education (2012007613000).

Notes and references

1 L. Moscou, in Introduction to Zeolite Science and Practice, Vol. 1 (Eds: H. Van Bekkum, E. M. Flanigen, P. A. Jacobs and J. C. Jansen), *Elsevier, Amsterdam, Stud. Surf. Sci. Catal*., 1991, pp. 58.
2 J. Kang, K. Cheng, L. Zhang, Q. Zhang, Q. Zhai and Y. Wang, *Angew. Chem. Int. Ed*., 2011, **50**, 5200.
3 J. Lu, C. Aydin, N. D. Browning and B. C. Gates, *Angew. Che Int. Ed*., 2012, **51**, 5842.
4 Y. Wu, J. Wang, P. Liu, W. Zhang, J. Gu and X. Wang, *J. Am Chem. Soc*., 2010, **132**, 17989.
5 B. Peng, Y. Yao, C. Zhao and J. A. Lercher, *Angew. Chem. Int. Ed*., 2012, **51**, 2072.
6 W. Song, C Zhao and J. A. Lercher, *Chem. Eur. J*., 2013, **19**, 9833.
7 B. Peng, X. Yuan, C. Zhao and J. A. Lercher, *J. Am. Chem. Soc*., 2012, **134**, 9400.
8 S. K. Hashmi and G. J. Hutchings, *Angew. Chem. Int. Ed*., 2006, **45**, 7896.
9 J. Kim, S. Lee, K. Cho, K. Na, C. Lee and R. Ryoo, *ACS Catal*., 2014, **4**, 3919.
10 C. Zhao, S. Kasakov, J. He and J. A. Lercher, *J. Catal*., **2012** 296, 12.
11 C. Zhao and J. A. Lercher, *Angew. Chem. Int. Ed*., 2012, **51**, 5935.
12 R. Nares, J. Ramírez, A. Gutiérrez-Alejandre, C. Louis and Klimova, *J. Phys. Chem*., *B*, 2002, **106**, 13287.
13 M. A. Keane, *Micro. Mater*., 1994, **3**, 93.
14 K. Tohji, Y. Udagawa, S. Tanabe and A. Ueno, *J. Am. Chem Soc*., 1984, **106**, 612.
15 M. A. Cauqui and J. M. Rodriguez-Izquierdo, *J. Non-Cryst. Solids*, 1992, 147-148, 724-738.
16 L. A. M. Hermans and J. W. Geus in Preparation of Catalysts (Eds.: B. Delmon, P. Grange, P. A. Jacobs and G. Poncelet), *Elsevier, Amsterdam*, 1979, pp. 113.
17 W. Song, Y. Liu, E. Baráth, C Zhao and J. A. Lercher, *Green Chem*., 2015, **17**, 1204.
18 P. Burattin, M. Che and C. Louis, *J. Phys, Chem., B*, 1997, **10** 7060.
19 P. Burattin, M. Che and C. Louis, *J. Phys, Chem., B*, 1998, **102** 2722.
20 H. G. Peng, L. Xu, H. H. Wu, K. Zhang and P. Wu, *Chem. Commun*., 2013, **49,** 2709.
21 X. Qian, J. Du, B. Li, M. Si, Y. Yang, Y. Hu, G. Niu, Y. Zhang, H Xu, B. Tu, Y. Tang and D. Zhao, *Chem. Sci*., 2011, **2**, 2006.
22 R. Jin, Y. Yang, Y. Li, L. Fang, Y. Xing and S. Song, *Chem Commun*., 2014, **50**, 5447.
23 D. Chen, L. L. Li, F. Q. Tang and S. Qi, *Adv. Mater*., 2009, **21**, 3804.
24 V. Valtchev, G. Majano, S. Mintova and J. Pérez-Ramírez, *Chem. Soc. Rev*., 2013, **42**, 263.
25 D. Verboekend and J. Pérez-Ramírez, *Catal. Sci. Technol*., 2011, **1**, 879.
26 R. Jin, Y. Yang, Y. Xing, L. Chen, S. Song and R. Jin, *ACS Nano*, 2014, **8**, 3664.
27 D. Wang, L. Xu and P. Wu, *J. Mater. Chem., A,* 2014, **2**, 1553
28 Z. Guo, F. Du, G. Li and Z. Cui, *Chem. Commun*., 2008, **25** 2911.
29 P. Jin, Q. Chen, L. Hao, R. Tian, L. Zhang and L. Wang, *J. Phys. Chem., B*, 2004, **108**, 6311.
30 S. He, C. Li, H. Chen, D. Su, B. Zhang, X. Cao, B. Wang, M. Wei, D. G. Evans and X. Duan, *Chem. Mater*., 2013, **25**, 1040.
31 E. N. Korytkova, A. V. Maslov, L. N. Pivovarova, Yu. V. Polegotchenkova, V. F. Povinich and V. V. Gusarov, *Inorg. Mater*., 2005, **41**, 743.
32 S. He, C. Li, H. Chen, D. Su, B. Zhang, X. Cao, B. Wang, M. Wei, D. G. Evans and X. Duan, *Chem. Mater*., 2013, **25**, 1040.
33 B. I. Mosqueda-Jimenez, A. Jentys, K. Seshan and J.A. Lercher, *J. catal*., 2003, **218**, 348.